

Supporting Information

Superhydrophilic metal-organic framework thin film for enhancing capillary-driven boiling heat transfer

Guang Yang,^{a,†} Juan Liu,^{b,†} Xin Cheng,^a Ye Wang,^a Xu Chu,^c Soumya Mukherjee,^b Alexandros Terzis,^d Andreas Schneemann,^e Weijin Li,^{b,} Jingyi Wu,^{a,*} and Roland A. Fischer^{b,*}*

^aSchool of Mechanical Engineering, Shanghai Jiao Tong University, Dongchuan Road 800, Shanghai 200240, China. E-mail: jywu@sjtu.edu.cn

^bChair of Inorganic and Metal-organic Chemistry, Catalysis Research Center & Department of Chemistry, Technical University of Munich, Lichtenbergstraße 4, 85748 Garching b. München, Germany. E-mail: roland.fischer@tum.de; wj.li@tum.de

^cCluster of Excellence SimTech, University of Stuttgart, Pfaffenwaldring 5a, 70569 Stuttgart, Germany.

^dFaculty of Aerospace Engineering, Technion Israel Institute of Technology, 3200003 Haifa, Israel

^eTechnische Universität Dresden, Bergstr. 66, 01069 Dresden, Germany

[†]These authors contributed to this work equally.

Contents

| | |
|---|----|
| 1. Chemicals and Materials..... | 4 |
| 2. Instruments and characterizations..... | 4 |
| 3. Supporting Figures..... | 6 |
| Figure S1. Porous view of the HKUST-1 structure along the crystallographic <i>c</i> axis. | 6 |
| Figure S2. Schematic illustration of a two-electrode system used for electrochemically depositing the HKUST-1 films. | 6 |
| Figure S3. Water adsorption isotherm measured on the powder HKUST-1 under 298.15 K. ... | 7 |
| Figure S4. GIXRD diffractogram of the prepared HKUST-1 film..... | 7 |
| Figure S5. The HKUST-1 film prepared by reacting 30 min with a solution of 1 g H ₃ TMA at: a) 1 V; b) under high magnifications of (a); c) 3 V; d) 5 V; e) 7 V; f) 10 V. | 9 |
| Figure S6. HKUST-1 films prepared by applying 5 V upon reacting 30 min using different concentrations of H ₃ TMA (in 100 g ethanol/water solution): a) 0.5 g; b) 1 g; c) 2 g; d) 3 g. | 10 |
| Figure S7. HKUST-1 films prepared by applying 5 V with a concentration of H ₃ TMA (1 g in 100 g ethanol/water) after reacting over different durations: a) 30 min; b) 60 min; c) 90 min; d) 120 min; e) 150 min; f) 180 min..... | 11 |
| Figure S8. (a) Photograph of our in-house experimental vapor chamber; (b) The dimensions of the heater-thermocouple block assembly inside the test chamber; (c) 3D view of the sample holder assembly; (d) Section view of the sample holder assembly.. | 12 |
| Figure S9. Validation of present experiments for capillary-driven boiling heat transfer by comparison with experimental data from the literature. | 13 |
| Figure S10. Schematics illustrating the fabrication procedures of the (a) multilayered and (b) chemical etched meshes. | 14 |
| Figure S11. Representative images from Camera #1 and Camera #2 during the wicking process in the pre-heated HKUST-1@Cu mesh. The micro front and the liquid height in the capillary tube were determined by the side-view Camera #2, considering that only a single liquid meniscus between the copper wires could reflect the backlight..... | 15 |
| Figure S12. Thermal images and temperature profiles during wicking with the HKUST-1@Cu mesh based porous structures on a substrate heated to 100 °C by infrared camera. The grey zone in (b) represents the capillary tube. | 16 |
| Figure S13. PXRD patterns of water-immersed HKUST-1 powder after treating each post-immersion sample at 85 °C. Despite surface leaching, under water immersion, its structural integrity is retained for at least 180 min, suggesting its stability during the wicking tests. | 17 |
| 4. Supporting tables | 18 |
| Table S1. Effective porosities of Cu mesh and HKUST-1@Cu mesh with different growth times..... | 18 |
| Table S2. Developments in the evaporator wicks for enhanced heat transfer (Heat source area: 10 mm×10 mm, working fluid: water)..... | 18 |
| Table S3. Comparison of the capillary wicking capability of HKUST-1@Cu mesh with reported data (working fluid: water)..... | 19 |
| 5. Supporting equations | 20 |
| 5.1 Wicking model on porous surface intaking from a capillary tube..... | 20 |
| 5.2 The calculation of saturation wetting front..... | 20 |

| | |
|--------------------------------|----|
| 6. Supporting videos | 21 |
| 7. Supporting references | 22 |

1. Chemicals and Materials

Copper meshes were purchased from G. Bopp + Co. AG , Trimesic acid (H₃TMA) was obtained from abcr GmbH. Ethanol (99.96%) was purchased from VWR. Tributylmethylammonium methyl sulfate (MBTS, ≥95%) was purchased from Santa Cruz Biotechnology. Ultrapure water (18.2 MΩ cm) was obtained from Millipore System.

2. Instruments and characterizations

Electrochemical deposition experiments were carried out on Metrohm Autolab potentiostat equipped with two-electrode system.

Grazing incidence X-ray diffraction (GIXRD) was performed on an X'pert PRO PANalytical instrument at room temperature (Bragg-Brentano geometry with fixed divergence slits, continuous mode, position sensitive detector, Ni filter, Cu Ka radiation, range $2\theta = 5-35^\circ$, step size 0.01313° , accumulation time 445 s per step). Powder X-ray diffraction (PXRD) patterns for powder samples were collected on a zero background disk equipped silicon wafer.

Scanning electron microscopy (SEM) images were collected on a Zeiss Navision 40 FIB SEM instrument (Carl Zeiss AG) with an accelerating voltage of 5 kV and a working distance of 6.5 ~7.5 mm.

Water vapour adsorption experiments were performed at 298K on a BELSORP-max instrument (Microtrac BEL, Japan). The water (fully deionized) was degassed via three freeze-pump-thaw cycles. Prior to the measurements the samples were activated by evacuation at 120 °C for 24 hours.

Optical images of dynamic wetting were recorded by NAC GX3, with a recording speed of 2000 fps, and IDS-UI-3180CP, with a recording speed of 240 fps.

Thermal images were recorded by an infrared camera (FLIR T630SC) with the resolution of 640×480 and an acquisition frame rate of 30Hz.

Measurement of effective porosity: Buoyancy method was utilized to measure the effective porosity of the mesh samples. First, the dry weights of the test samples ($m_{air, dry}$) were measured in air after placing them in a vacuum oven at 80 °C for 1 hour. Prior to the submerged weight measurements, the mesh samples were degassed under vacuum. The samples were put into a container filled with water, placed in a vacuum oven for 1 hour to allow the gas to effuse. Then the saturated sample was immersed in the beaker filled with water and hung on an electronic balance (Sartorius QUINTIX224-1CN, readability 0.1 mg). The data acquisition device recorded the weight of the saturated sample with a precision of ±0.1 mg as soon as the balance readout was stabilized. Submerged weights of the saturated samples ($m_{submerged}$) were measured three times for each sample to minimize experimental errors. By measuring the weights of the mesh samples, volume of the solid is calculated as follows:

$$V_{solid} = \frac{m_{air, dry} - m_{submerged}}{\rho_l}$$

where ρ_l is the fluid density. Finally, the effective porosity, defined as the volumetric fraction of the void space, can be determined as follows:

$$\varphi = 1 - \frac{V_{solid}}{V_{total}} = 1 - \frac{m_{air, dry} - m_{submerged}}{\rho_l HW\delta}$$

H , W , δ are the height, width and thickness of the sample, respectively. Due to the high microporosity^[1,2] of HKUST-1, effective porosity of the copper mesh remains nearly unchanged after coating (**Table S1**).

Fabrication of multi-layer mesh: Multilayer meshes and the connections between a copper mesh with a copper plate were manipulated by diffusion bonding. Detailed manufacturing processes are presented in **Figures S8**. First, the copper meshes/plates were cleaned by dilute hydrochloric acid (2 moles/L) for 3 minutes and then flushed in deionized (DI) water to remove the copper oxide surface. The cleaned meshes/plates were stacked together between graphite plates. Then, the meshes/plates were clamped by a 3 kg weight and placed in a high-temperature vacuum oven at 950 °C for 2 hours to form the robust structures.^[3]

Fabrication of chemical-etched mesh: Etched nanoscale structures were fabricated on the wire surfaces by chemical etching. Copper meshes were dipped in an alkaline solution composed of NaClO₂, NaOH, Na₂PO₄·12H₂O and DI water (wt/wt/wt/wt, 3.75:5:10:100) to obtain high surface roughness. After conducting oxidation at 96 °C for 15 minutes, high-density nano-grasses were formed on the etched meshes. The SEM image of the etched mesh refers to our previous study.⁴

3. Supporting Figures

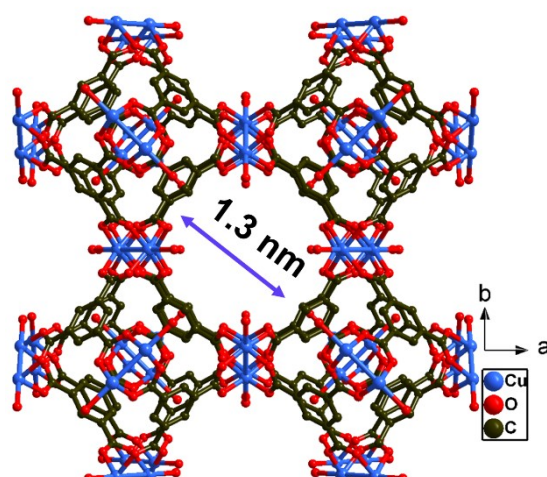


Figure S1. Porous view of the HKUST-1 structure along the crystallographic *c* axis.

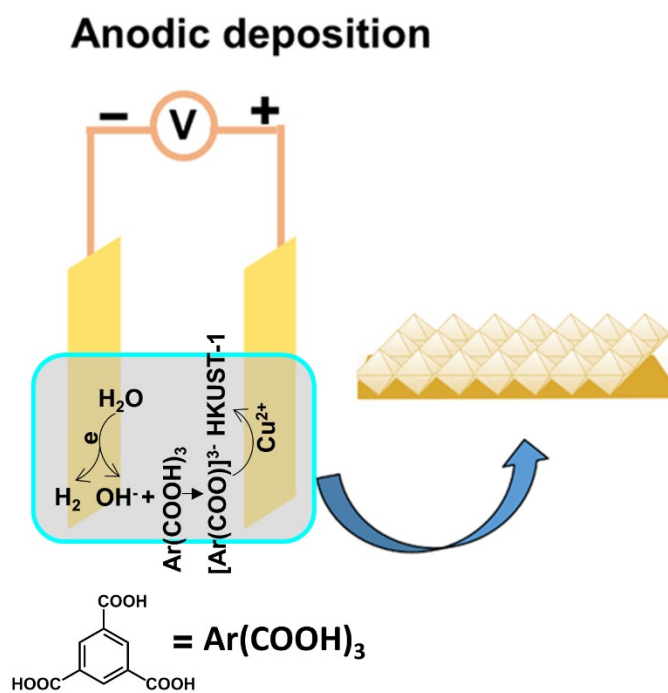


Figure S2. Schematic illustration of a two-electrode system used for electrochemically depositing the HKUST-1 films.

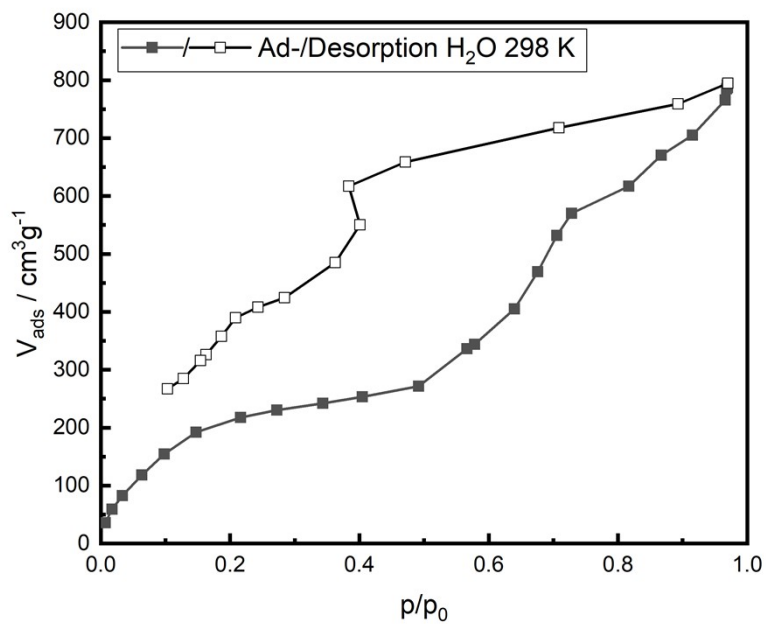


Figure S3. Water adsorption isotherm measured on the powder HKUST-1 under 298.15 K. The result suggested that HKUST-1 exhibits high water uptake under ambient conditions

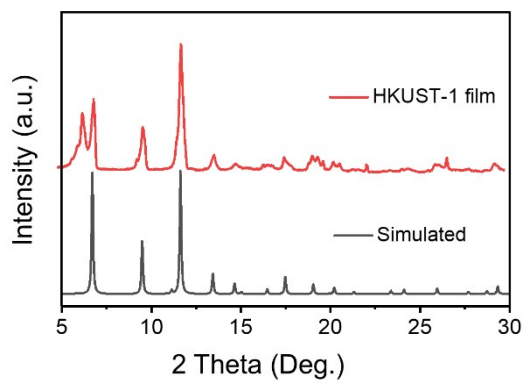


Figure S4. GIXRD diffractogram of the prepared HKUST-1 film.

S5-S7. Morphology and thickness study of HKUST-1 films.

The morphology and film thickness of the obtained HKUST-1 films were studied by tailoring the voltage, concentration of the organic linker H₃TMA and reaction time. As shown in **Figure S5**, only a small amount of HKUST-1 crystallites with an average size of ~180 nm, was randomly grown on the copper mesh surface when applying a voltage of 1 V. Through increasing the voltage from 2 V to 10 V, a series of HKUST-1 films (which demonstrated good coalescence of microcrystals with small intergranular voids) were grown on copper mesh. The HKUST-1 crystallite sizes exhibited a range of ~14.3 μm, ~13.5 μm, ~12.1 μm and ~9.6 μm with corresponding thicknesses of ~3.9 μm, ~4.3 μm, ~4.0 μm, ~4.5 μm for films prepared at 2 V, 3 V, 5 V, 7 V and 10 V, respectively. However, by applying high voltages (e.g., 7 V and 10 V) for growing the films, copper meshes get severely corroded to become brittle, therefore easy to be broken for further use while under low voltage (e.g., 1 V, 2 V and 3 V). As a result, large sized copper meshes cannot be covered. Therefore, we select the voltage of 5 V for further preparing the HKUST-1 film. As shown in **Figure S6**, in the electrolytes comprised of 0.5 g H₃TMA in 100 g ethanol/water (v/v, 1:1), the HKUST-1 crystallites were randomly and non-homogeneously distributed on the copper meshes. Surface of the copper mesh was found partially covered with small sized (< 500 nm) HKUST-1 crystallites; whereas other parts of the surface were found covered with larger sized (~11.7 μm) HKUST-1 crystallites (**Figure S6a**). When increasing the concentration of H₃TMA from 0.0005 g/g to 0.01 g/g, HKUST-1 was found uniformly and homogeneously packed on the surface of copper mesh (**Figure S6b**). Increasing the concentration of H₃TMA to 0.02 g/g, the HKUST-1 crystallite size undergoes an increase to ~15.0 μm with the film thickness of ~5.7 μm (**Figure S6c**). When adding 0.03 g/g H₃TMA to the electrolyte, some HKUST-1 crystallites can be found to fall off from the copper mesh (**Figure S6d**). While growing the HKUST-1 films, to reduce the use of chemicals including the toxic electrolyte salt (MTBS), we use 0.01 g/g H₃TMA in the electrolyte solution. Thickness of the HKUST-1 films on the copper mesh plays a key role on the wettability of HKUST-1@Cu mesh and their capillary wicking performances. By controlling the reaction time, thickness of the obtained films can be tuned from ~4.0 μm (30 min), ~6.3 μm (60 min), ~11.8 μm (90 min), ~14.4 μm (120 min), ~11.5 μm (150 min) and ~13.9 μm (180 min) (**Figure S7**). Over long reaction times (150 min and 180 min), the macropores of the copper substrate are blocked by the HKUST-1 crystallites. Therefore, we only screened the capillary wicking performances of the HKUST-1 film prepared by applying 5 V for the reaction times of 30 min, 60 min, 90 min and 120 min with 0.01 g/g H₃TMA in the electrolyte solution (**Figure 1f**).

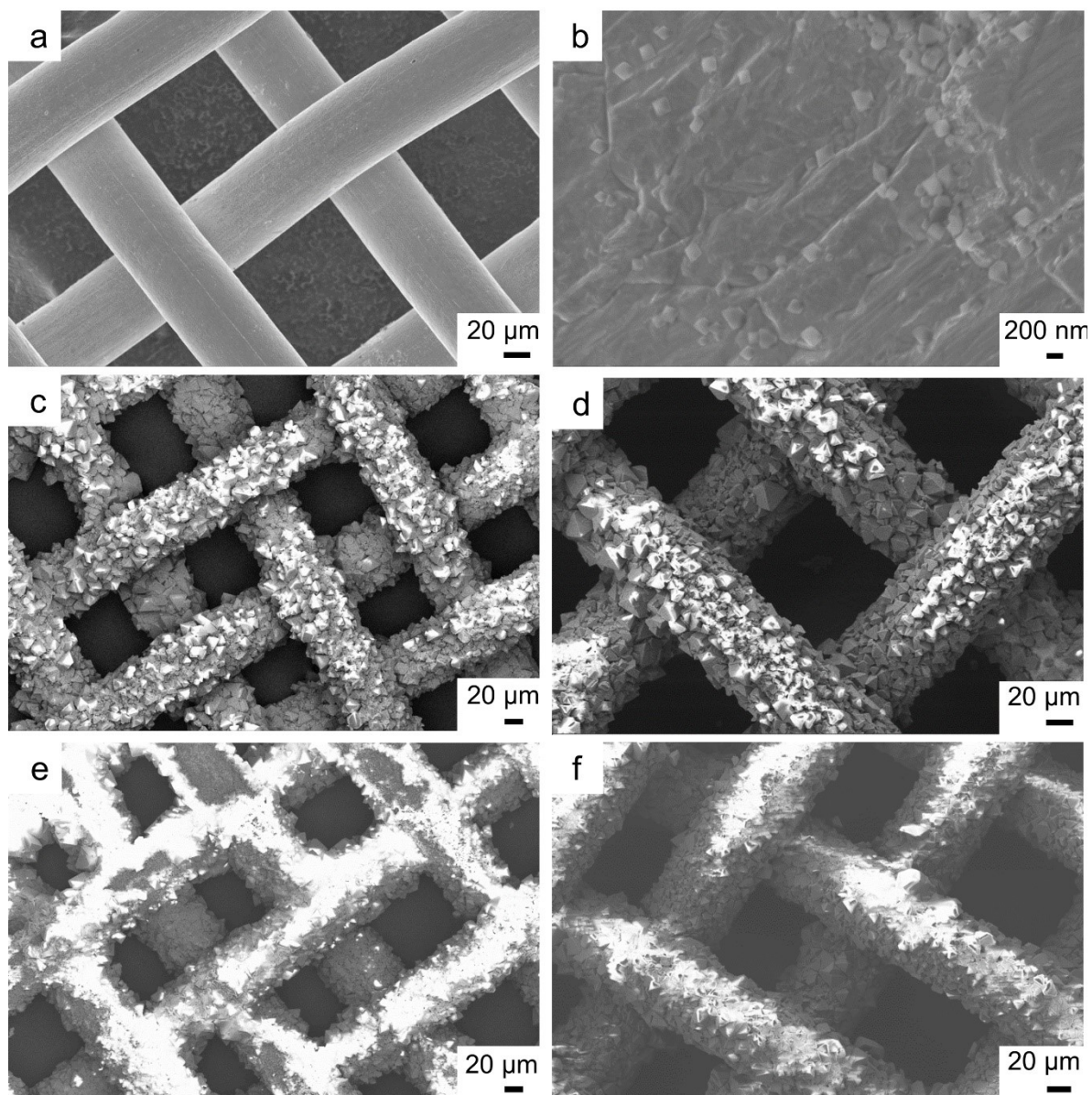


Figure S5. The HKUST-1 film prepared by reacting 30 min with a solution of 1 g H₃TMA at: a) 1 V; b) under high magnifications of (a); c) 3 V; d) 5 V; e) 7 V; f) 10 V.

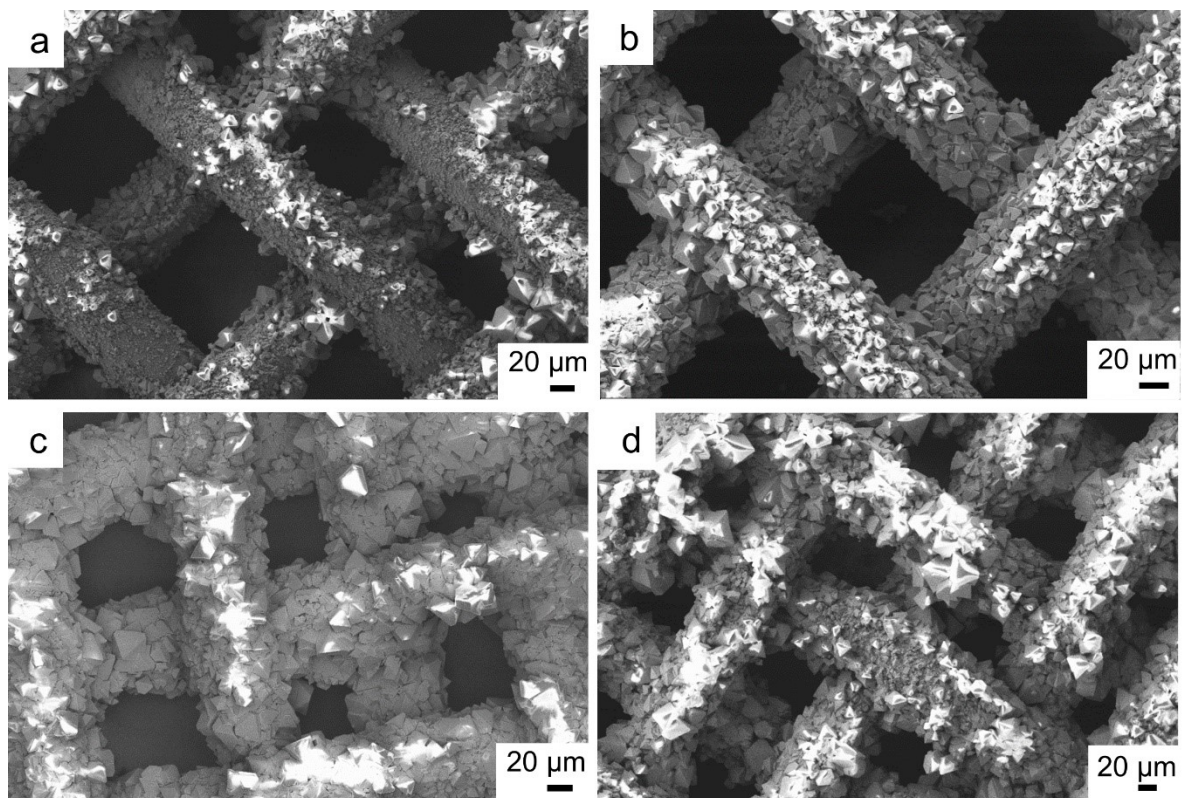


Figure S6. HKUST-1 films prepared by applying 5 V upon reacting 30 min using different concentrations of H₃TMA (in 100 g ethanol/water solution): a) 0.5 g; b) 1 g; c) 2 g; d) 3 g.

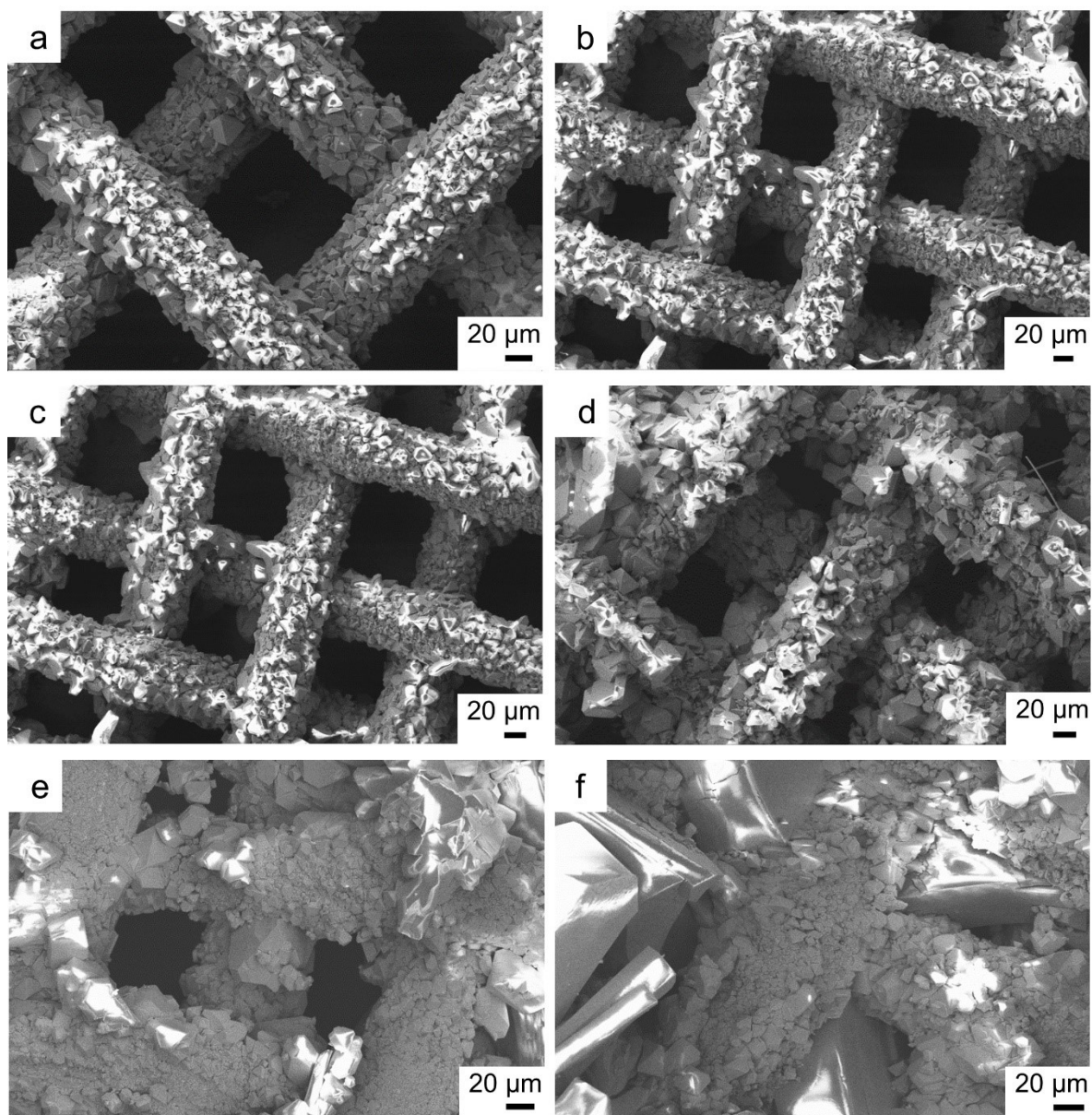


Figure S7. HKUST-1 films prepared by applying 5 V with a concentration of H₃TMA (1 g in 100 g ethanol/water) after reacting over different durations: a) 30 min; b) 60 min; c) 90 min; d) 120 min; e) 150 min; f) 180 min.

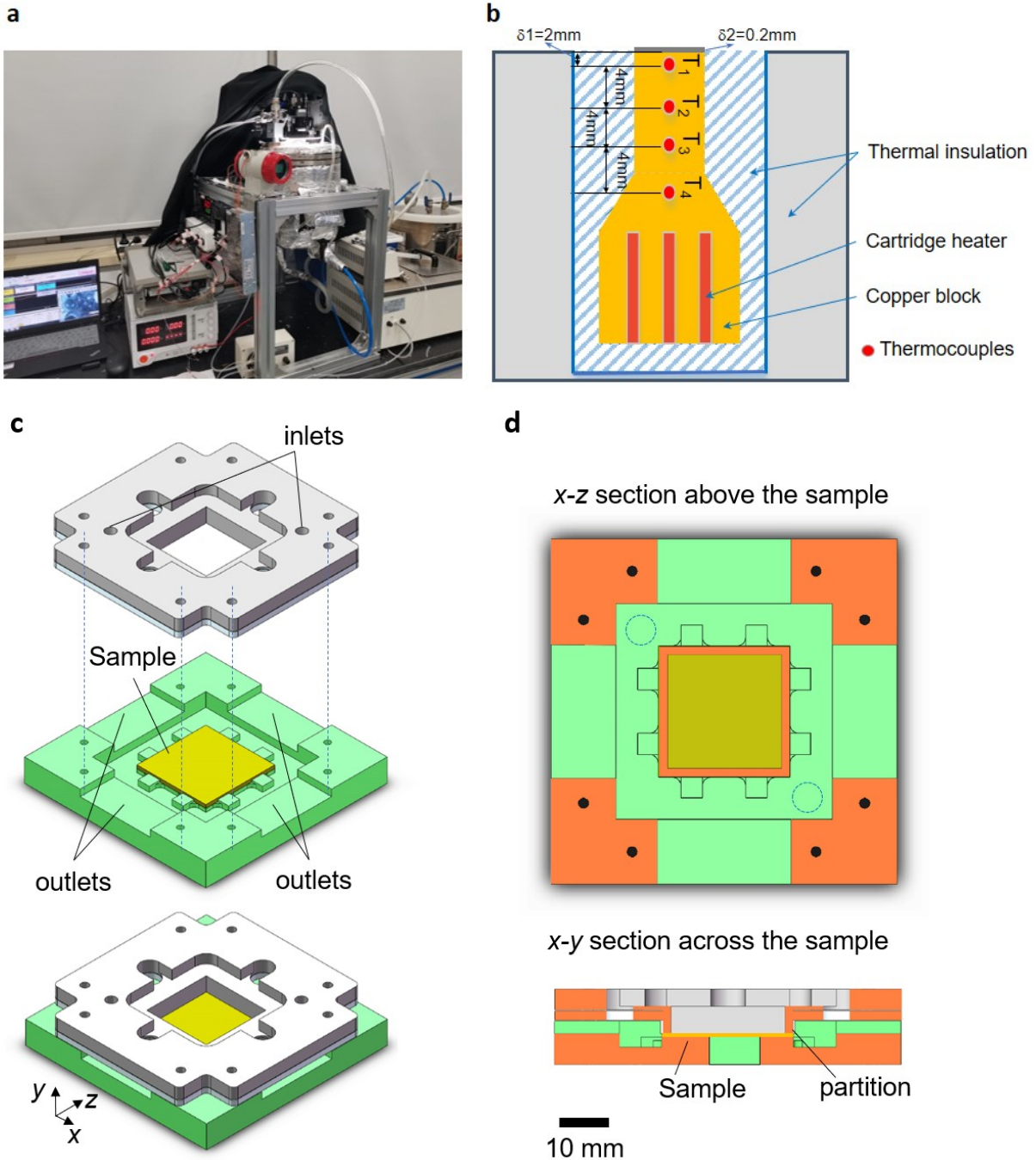


Figure S8. (a) Photograph of our in-house experimental vapor chamber; (b) The dimensions of the heater-thermocouple block assembly inside the test chamber; (c) 3D view of the sample holder assembly; (d) Section view of the sample holder assembly. Heights of the four outlets reside at the same level as the top surface of the sample. The sample is also protected by partitions to prevent water flooding, therefore the water within the porous wick is exclusively supplied in a passive manner by the capillary wicking mechanism.

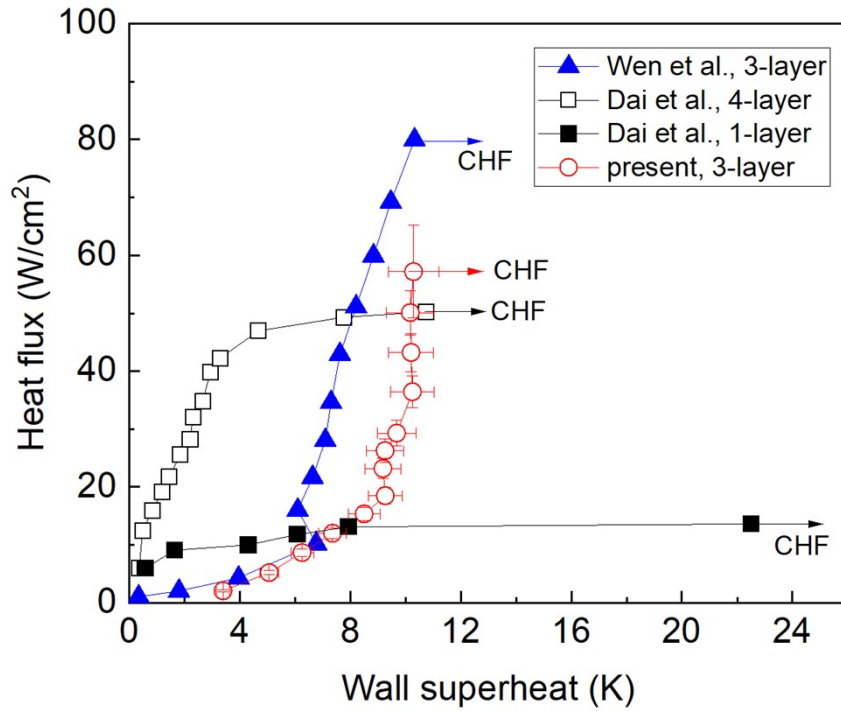


Figure S9. Validation of present experiments for capillary-driven boiling heat transfer by comparing to experimental data from the literature. For a 3-layer copper mesh, our results are in agreement with those from Wen et al.[9] with the difference in wall superheat below 3K for a given heat flux. Heat transfer curves for 1-layer and 4-layer meshes from Dai et al.[8] are also included. Though the results for 3-layer mesh were not reported in their study, it can be inferred that the data of 3-layer mesh should fall in between the curves of those corresponding to 1-layer and 4-layer meshes. Also, the determined CHF for 3-layer mesh falls between that reported by Wen et al. [9] and Dai et al. [8]. (Data from references were extracted using the OriginPro software.)

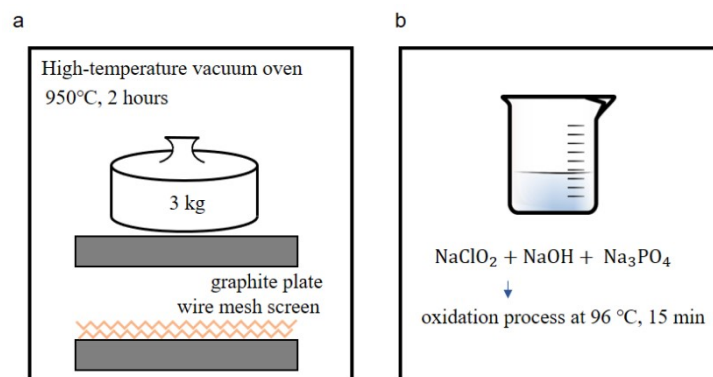


Figure S10. Schematics illustrating the fabrication procedures of the (a) multilayered and (b) chemical etched meshes.

S11. Identification of the nano and micro wetting fronts

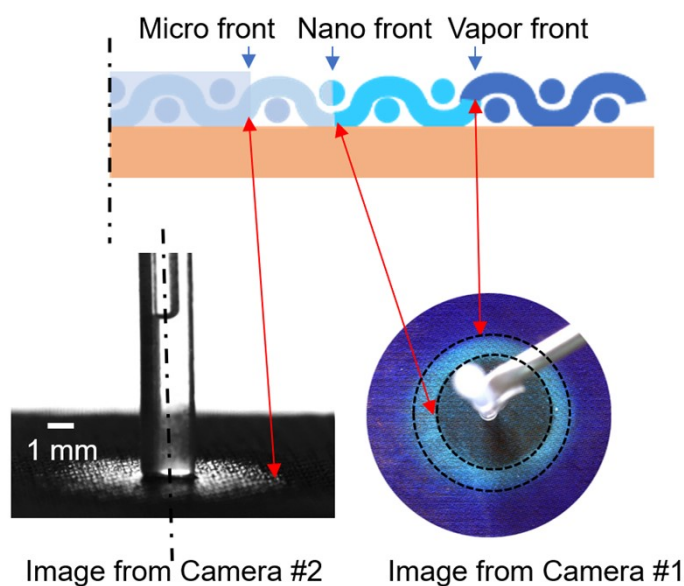


Figure S11. Representative images from Camera #1 and Camera #2 during the wicking process in the pre-heated HKUST-1@Cu mesh. The micro front and the liquid height in the capillary tube were determined by the side-view Camera #2, considering that only a single liquid meniscus between the copper wires could reflect the backlight.^[5] Since the inner diameter of the capillary tube remained constant, the amount of wicked liquid can be calculated directly from the liquid height. The nano front and the vapour front (not exist in the unheated wicking condition of Figure 4b) were determined by the top-view Camera #1, according to the clear distinction between different colours.

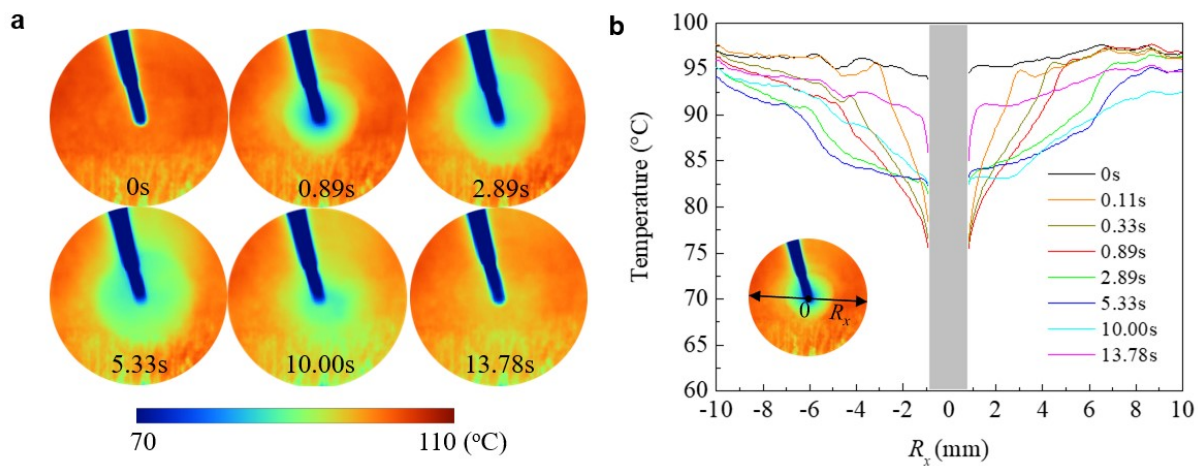


Figure S12. Thermal images and temperature profiles during wicking with the HKUST-1@Cu mesh based porous structures on a substrate heated to 100 °C by infrared camera. The grey zone in (b) represents the capillary tube.

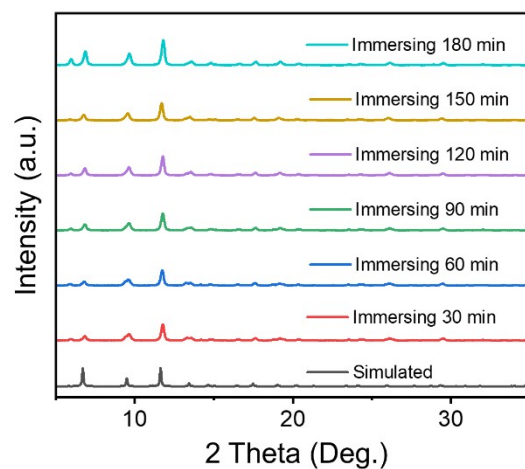


Figure S13. PXRD patterns of water-immersed HKUST-1 powder after treating each post-immersion sample at 85 °C. Despite surface leaching, under water immersion, its structural integrity is retained for at least 180 min, suggesting its stability during the wicking tests.

4. Supporting tables

Table S1. Effective porosities of Cu mesh and HKUST-1@Cu mesh with different growth times

| | Bare Cu mesh | 30 min | 60 min | 90 min | 120 min |
|------------------------|--------------|-------------|-------------|-------------|-------------|
| Effective porosity (-) | 0.61 ± 0.01 | 0.61 ± 0.01 | 0.60 ± 0.01 | 0.57 ± 0.01 | 0.57 ± 0.01 |

Table S2. Developments in the evaporator wicks for enhanced heat transfer (Heat source area: 10 mm×10 mm, working fluid: water)

| Structure type of the wick | CHF (W/cm ²) | HTC@CHF (kW/(m ² K)) | References |
|--|--|---|-------------------------|
| 3-layer Copper mesh, HKUST-1@Cu mesh | 169.9 (increased by 205% compared to mesh) | 104.7 (increased by 90% compared to mesh) | This work |
| Silicon micropillars | 40-50 | 20-25 | Adera <i>et al.</i> [6] |
| Carbon nanotubes | 130–140 | 60–80 | Cai <i>et al.</i> [7] |
| Copper mesh, composite with microchannel | 152.2 | 91 | Dai <i>et al.</i> [8] |
| Copper mesh, chemical etching and cleaning | 3-layer: 145.7 (increased by 82.1% compared to mesh) | 138.7 (increased by 70% compared to mesh) | Wen <i>et al.</i> [9] |

Table S3. Comparison of the capillary wicking capability of HKUST-1@Cu mesh with reported data (working fluid: water)

| Structure type | Average wicking speed $R/t^{0.5}$ (mm/s ^{0.5}) | References |
|---|--|------------------------------------|
| HKUST-1@Cu mesh | 6.4 | This work |
| Hierarchical structures with ZnO nanowires | 3.2 | Wang <i>et al.</i> ^[10] |
| Hierarchical structures with CuO nanocactuses | 3.3 | Lee <i>et al.</i> ^[11] |
| Silicon nanowires | 1.95 | Shim <i>et al.</i> ^[12] |
| Micronic spikes | 0.3 | Bico <i>et al.</i> ^[13] |

5. Supporting equations

5.1 Wicking model on porous surface intaking from a capillary tube

The radial capillary penetration of liquids into porous media is driven by the capillary pressure and resisted by the viscous pressure loss due to friction and evaporation.

$$P_c = P_\mu + P_m \quad (S1)$$

P_c is the capillary pressure, and is estimated from the Young-Laplace equation,

$$P_c = \frac{2\sigma\cos\theta}{R_{eff}} \quad (S2)$$

where θ is the contact angle between solid and liquid, R_{eff} is the equivalent capillary. For composite porous structures, R_{eff} can be considered as series and parallel connection of the pores of varying sizes.

By considering laminar and incompressible flow, the Darcy's law for the liquid flow can be expressed as,

$$u_R = -\frac{K\partial P_\mu}{\mu\partial R} \quad (S3)$$

K is the permeability of the porous material; R is the radius of the wetted region. u_R is the radial Darcy velocity at radius R . By integration

$$P_\mu = \frac{\mu\varphi}{K}R\ln\left(\frac{R}{R_{in}}\right)\frac{\partial R}{\partial t} \quad (S4)$$

R_{in} is the wicking radius at the initial time, and R is the wicking radius at current moment.

Assuming that the evaporation rate stays constant and uniform in the penetration region, the viscous pressure loss P_m could be approximately expressed as^[14]

$$P_m = \frac{1\mu\dot{m}_e}{4K\rho H}\left[2R^2\ln\left(\frac{R}{R_{in}}\right) - (R^2 - R_{in}^2)\right] \quad (S5)$$

\dot{m}_e is the equivalent evaporation rate [kg/m²s] on top surface of the porous layer. H is the effective thickness of the porous layer.

Combining Equations S1, S2, S4 and S5 yield

$$\frac{2\sigma\cos\theta}{R_{eff}} = \frac{\mu\varphi}{K}R\ln\left(\frac{R}{R_{in}}\right)\frac{\partial R}{\partial t} + \frac{1\mu\dot{m}_e}{4K\rho H}\left[2R^2\ln\left(\frac{R}{R_{in}}\right) - (R^2 - R_{in}^2)\right] \quad (S6)$$

It is therefore inferred from Equation S6, that the evaporation effect acts as a resistance to the capillary penetration process.

5.2 The calculation of saturation wetting front

For the cases without evaporation, *i.e.* $\dot{m}_e=0$, **Equation S6** reduces to

$$\frac{2\sigma\cos\theta}{R_{eff}} = \frac{\mu\varphi}{K}R\ln\left(\frac{R}{R_{in}}\right)\frac{\partial R}{\partial t} \quad (S7)$$

Based on **Equations S3** and **S7**, the instantaneous volumetric flow rate, $q(t)$, is determined from the wetting radius,

$$q(t) = \frac{2\pi KH}{\mu\ln\frac{R(t)}{R_{in}}} \frac{2\sigma\cos\theta}{R_{eff}} \quad (S8)$$

However, the liquid behaves in a hierarchical flow in the composite HKUST-1@Cu mesh porous structure. $R(t)$ in **Equations S7** and **S8** are not the actual wetting fronts, as both nano and micro fronts exist in the wicking, but an equivalent wetting radius R_{sa} that assumes that the fluid flows when saturated. Due to unsaturated nature of the flow, the actual wetting radius should be larger than R_{sa} .

Since the instantaneous volumetric flow rate, $q(t)$, can also be determined from the liquid volume in the capillary tube ($q(t) = dV_{out}/dt$), the saturated wetting radius can be obtained from the following equation,

$$\pi(R_{sa}(t)^2 - R_{in}^2)H\phi = q(t) = dV_{out}/dt \quad (S9)$$

6. Supporting videos

Video S1. Drying of the HKUST-1@Cu porous structures at the heat flux of 170 W/cm².

Video S2. Isothermal wicking in the HKUST-1@Cu mesh (video from Camera #2).

Video S3. Isothermal wicking in the HKUST-1@Cu mesh (video from Camera #1).

Video S4. Wicking and evaporation in the heated HKUST-1@Cu mesh (video from Camera #1).

Video S5. Capillary boiling on the bare copper porous structures at the heat input of 40 W/cm².

Video S6. Capillary boiling on the HKUST-1@Cu mesh porous structures at the heat input of 100 W/cm².

7. Supporting references

- 1 S.S.Y. Chui, *Science*, 1999, **283**, 1148–1150
- 2 D.Q.Y. Z. F. Ju, *Chinese J. Inorg. Chem.*, 2013, **29**, 1633.
- 3 M. Eroglu, T.I. Khan, N. Orhan, *Mater. Sci. Technol.*, 2002, **18**, 68–72.
- 4 Y. Wang, Y. Lin, G. Yang, J. Wu, *Langmuir*, 2021, **37**, 2289–2297.
- 5 A.M. Emelyanenko, L.B. Boinovich, K.A. Emelyanenko, *J. Colloid Interface Sci.*, 2020, **567**, 224–234.
- 6 S. Adera, D. Antao, R. Raj, E.N. Wang, *Int. J. Heat Mass Transf.*, 2016, **101**, 280–294.
- 7 Q. Cai, A. Bhunia, *Int. J. Heat Mass Transf.*, 2012, **55**, 5544–5551..
- 8 X. Dai, F. Yang, R. Yang, Y.-C. Lee, C. Li, *Int. J. Heat Mass Transf.*, 2013, **64**, 1101–1108..
- 9 R. Wen, S. Xu, Y. C. Lee, R. Yang, *Nano Energy*, 2018, **51**, 373-382.
- 10 Z. Wang, J. Zhao, A. Bagal, E.C. Dandley, C.J. Oldham, T. Fang, G.N. Parsons, C.-H. Chang, *Langmuir*, 2016, **32**, 8029–8033.
- 11 J. Lee, Y. Suh, P.P. Dubey, M.T. Barako, Y. Won, *ACS Appl. Mater. Interfaces*, 2019, **11**, 1546–1554.
- 12 D. Il Shim, G. Choi, N. Lee, T. Kim, B.S. Kim, H.H. Cho, *ACS Appl. Mater. Interfaces*, 2017, **9**, 17595–17602.
- 13 J. Bico, C. Tordeux, D. Quéré, *Europhys. Lett.*, 2001, **55**, 214–220.
- 14 M. Liu, J. Wu, Y. Gan, D.A.H. Hanaor, C.Q. Chen, *Langmuir*, 2016, **32**, 9899–9904.